Mid-infrared Raman-soliton continuum pumped by a nanotube-mode-locked sub-picosecond Tm-doped MOPFA

M. Zhang,[1,*] E. J. R. Kelleher,[1] T. H. Runcorn,[1] V. M. Mashinsky,[2] O. I. Medvedkov,[2] E. M. Dianov,[2] D. Popa,[3] S. Milana,[3] T. Hasan,[3] Z. Sun,[3] F. Bonaccorso,[3,4] Z. Jiang,[3] E. Flahaut,[5,6] B. H. Chapman,[1] A. C. Ferrari,[3] S. V. Popov[1] and J. R. Taylor[1]

[1]*Femtosecond Optics Group, Department of Physics, Imperial College London, London, SW7 2AZ, UK*
[2]*Fiber Optics Research Center, General Physics Institute, Moscow, 119333, Russian Federal, Russia*
[3]*Cambridge Graphene Centre, University of Cambridge, 9 JJ Thomson Avenue, Cambridge, CB3 0FA, UK*
[4]*CNR IPCF Istituto per i Processi Chimico-Fisici, Viale F. Stagno D'Alcontres 37, I-98158 Messina, Italy*
[5]*Universitéde Toulouse; UPS, INP; Institut Carnot CIRIMAT, 118 route de Narbonne, F-31062 Toulouse cedex 9, France*
[6]*CNRS; Institut Carnot CIRIMAT, F-31062 Toulouse, France*
[*]*m.zhang10@imperial.ac.uk*

Abstract: We demonstrate a mid-infrared Raman-soliton continuum extending from 1.9 to 3 μm in a highly germanium-doped silica-clad fiber, pumped by a nanotube mode-locked thulium-doped fiber system, delivering 12 kW sub-picosecond pulses at 1.95 μm. This simple and robust source of light covers a portion of the atmospheric transmission window.

OCIS codes: (140.4050) Mode-locked lasers; (160.4236) Nanomaterials; (190.4370) Nonlinear optics, fibers.

References and links

J. M. Dudley and J. R. Taylor, "Ten years of nonlinear optics in photonic crystal fibre," Nat. Photonics 3(2), 85–90 (2009).
2. A. Kudlinski, G. Bouwmans, O. Vanvincq, Y. Quiquempois, A. Le Rouge, L. Bigot, G. Mélin, and A. Mussot, "White-light cw-pumped supercontinuum generation in highly GeO_2-doped-core photonic crystal fibers," Opt. Lett. **34**(23), 3631–3633 (2009).
3. K. K. Chen, S. U. Alam, J. H. V. Price, J. R. Hayes, D. Lin, A. Malinowski, C. Codemard, D. Ghosh, M. Pal, S. K. Bhadra, and D. J. Richardson, "Picosecond fiber MOPA pumped supercontinuum source with 39 W output power," Opt. Express **18**(6), 5426–5432 (2010).
4. M. J. F. Digonnet, *Rare earth doped fiber lasers and amplifiers* (Marcel Dekker, New York, NY, USA, 1993).
5. O. Okhotnikov, *Fiber Lasers* (Wiley-VCH, Berlin, 2012).
6. A. Kudlinski, A. K. George, J. C. Knight, J. C. Travers, A. B. Rulkov, S. V. Popov, and J. R. Taylor, "Zero-dispersion wavelength decreasing photonic crystal fibers for ultraviolet-extended supercontinuum generation," Opt. Express **14**(12), 5715–5722 (2006).
7. P. Werle, F. Slemr, K. Maurer, R. Kormann, R. Mücke, and B. Jänker, "Near- and mid-infrared laser-optical sensors for gas analysis," Opt. Lasers Eng. **37**(2-3), 101–114 (2002).
8. L. Rimai, E. W. Kaiser, E. Schwab, and E. C. Lim, "Application of time-resolved infrared spectral photography to chemical kinetics," Appl. Opt. **31**(3), 350–357 (1992).
9. G. Sepp and R. Protz, "Laser beam source for a directional infrared countermeasures (DIRCM) weapon system," US 6587486 B1 (2003).
10. C. Xia, M. Kumar, M.-Y. Cheng, R. S. Hegde, M. N. Islam, A. Galvanauskas, H. G. Winful, F. L. Terry, Jr., M. J. Freeman, M. Poulain, and G. Mazé, "Power scalable mid-infrared supercontinuum generation in ZBLAN fluoride fibers with up to 1.3 watts time-averaged power," Opt. Express **15**(3), 865–871 (2007).
11. C. Xia, M. Kumar, O. P. Kulkarni, M. N. Islam, F. L. Terry, Jr., M. J. Freeman, M. Poulain, and G. Mazé, "Mid-infrared supercontinuum generation to 4.5 μm in ZBLAN fluoride fibers by nanosecond diode pumping," Opt. Lett. **31**(17), 2553–2555 (2006).
12. J. S. Sanghera, L. Brandon Shaw, and I. D. Aggarwal, "Chalcogenide Glass-Fiber-Based Mid-IR Sources and Applications," IEEE J. Sel. Top. Quantum Electron. **15**(1), 114–119 (2009).

#191514 - $15.00 USD Received 30 May 2013; revised 29 Jul 2013; accepted 29 Jul 2013; published 24 Sep 2013

13. O. P. Kulkarni, V. V. Alexander, M. Kumar, M. J. Freeman, M. N. Islam, J. F. L. Terry, Jr., M. Neelakandan, and A. Chan, "Supercontinuum generation from ~1.9 to 4.5 μm in ZBLAN fiber with high average power generation beyond 3.8 μm using a thulium-doped fiber amplifier," J. Opt. Soc. Am. B **28**(10), 2486–2498 (2011).
14. P. Domachuk, N. A. Wolchover, M. Cronin-Golomb, A. Wang, A. K. George, C. M. B. Cordeiro, J. C. Knight, and F. G. Omenetto, "Over 4000 nm bandwidth of mid-IR supercontinuum generation in sub-centimeter segments of highly nonlinear tellurite PCFs," Opt. Express **16**(10), 7161–7168 (2008).
15. M. Liao, C. Chaudhari, G. Qin, X. Yan, T. Suzuki, and Y. Ohishi, "Tellurite microstructure fibers with small hexagonal core for supercontinuum generation," Opt. Express **17**(14), 12174–12182 (2009).
16. J. H. V. Price, T. M. Monro, H. Ebendorff-Heidepriem, F. Poletti, P. Horak, V. Finazzi, J. Y. Y. Leong, P. Petropoulos, J. C. Flanagan, G. Brambilla, F. Xian, and D. J. Richardson, "Mid-IR Supercontinuum Generation From Nonsilica Microstructured Optical Fibers," IEEE J. Sel. Top. Quantum Electron. **13**(3), 738–749 (2007).
17. D. Ravaine and G. Perera, "Corrosion Studies of Various Heavy-Metal Fluoride Glasses in Liquid Water: Application to Fluoride-Ion-Selective Electrode," J. Am. Ceram. Soc. **69**(12), 852–857 (1986).
18. P. Lucas, M. A. Solis, D. L. Coq, C. Juncker, M. R. Riley, J. Collier, D. E. Boesewetter, C. Boussard-Plédel, and B. Bureau, "Infrared biosensors using hydrophobic chalcogenide fibers sensitized with live cells," Sensor Actuat," Sens. Actua. B. **119**, 355–362 (2006).
19. E. M. Dianov and V. M. Mashinsky, "Germania-based core optical fibers," J. Lightwave Technol. **23**(11), 3500–3508 (2005).
20. V. M. Mashinsky, V. B. Neustruev, V. V. Dvoyrin, S. A. Vasiliev, O. I. Medvedkov, I. A. Bufetov, A. V. Shubin, E. M. Dianov, A. N. Guryanov, V. F. Khopin, and M. Y. Salgansky, "Germania-glass-core silica-glass-cladding modified chemical-vapor deposition optical fibers: optical losses, photorefractivity, and Raman amplification," Opt. Lett. **29**(22), 2596–2598 (2004).
21. B. A. Cumberland, S. V. Popov, J. R. Taylor, O. I. Medvedkov, S. A. Vasiliev, and E. M. Dianov, "2.1 μm continuous-wave Raman laser in GeO_2 fiber," Opt. Lett. **32**(13), 1848–1850 (2007).
22. F. L. Galeener, J. J. C. Mikkelsen, R. H. Geils, and W. J. Mosby, "The relative Raman cross sections of vitreous SiO_2, GeO_2, B_2O_3, and P_2O_5," Appl. Phys. Lett. **32**(1), 34–36 (1978).
23. E. M. Dianov, I. A. Bufetov, V. M. Mashinsky, V. B. Neustruev, O. I. Medvedkov, A. V. Shubin, M. A. Melkumov, A. N. Gur'yanov, V. F. Khopin, and M. V. Yashkov, "Raman fibre lasers emitting at a wavelength above 2 μm," Quantum Electron. **34**(8), 695–697 (2004).
24. E. A. Anashkina, A. V. Andrianov, M. Y. Koptev, V. M. Mashinsky, S. V. Muravyev, and A. V. Kim, "Generating tunable optical pulses over the ultrabroad range of 1.6-2.5 μm in GeO_2-doped silica fibers with an Er:fiber laser source," Opt. Express **20**(24), 27102–27107 (2012).
25. V. A. Kamynin, A. S. Kurkov, and V. M. Mashinsky, "Supercontinuum generation up to 2.7 μm in the germanate-glass-core and silica-glass-caldding fiber," Laser Phys. Lett. **9**(3), 219–222 (2012).
26. C. Agger, C. Petersen, S. Dupont, H. Steffensen, J. K. Lyngsø, C. L. Thomsen, J. Thøgersen, S. R. Keiding, and O. Bang, "Supercontinuum generation in ZBLAN fibers-detailed comparison between measurement and simulation," J. Opt. Soc. Am. B **29**(4), 635–645 (2012).
27. W. Gao, M. El Amraoui, M. Liao, H. Kawashima, Z. Duan, D. Deng, T. Cheng, T. Suzuki, Y. Messaddeq, and Y. Ohishi, "Mid-infrared supercontinuum generation in a suspended-core As_2S_3 chalcogenide microstructured optical fiber," Opt. Express **21**(8), 9573–9583 (2013).
28. C. E. S. Castellani, E. J. R. Kelleher, D. Popa, T. Hasan, Z. Sun, A. C. Ferrari, S. V. Popov, and J. R. Taylor, "CW-pumped short pulsed 1.12 μm Raman laser using carbon nanotubes," Laser Phys. Lett. **10**(1), 015101 (2013).
29. Z. Sun, T. Hasan, and A. C. Ferrari, "Ultrafast lasers mode-locked by nanotubes and graphene," Physica E **44**(6), 1082–1091 (2012).
30. D. Popa, Z. Sun, T. Hasan, W. B. Cho, F. Wang, F. Torrisi, and A. C. Ferrari, "74-fs nanotube-mode-locked fiber laser," Appl. Phys. Lett. **101**(15), 153107 (2012).
31. T. Hasan, Z. Sun, F. Wang, F. Bonaccorso, P. H. Tan, A. G. Rozhin, and A. C. Ferrari, "Nanotube-Polymer Composites for Ultrafast Photonics," Adv. Mater. **21**(38â€“39), 3874–3899 (2009).
32. Z. Sun, A. G. Rozhin, F. Wang, T. Hasan, D. Popa, W. O'Neill, and A. C. Ferrari, "A compact, high power, ultrafast laser mode-locked by carbon nanotubes," Appl. Phys. Lett. **95**(25), 253102 (2009).
33. F. Wang, A. G. Rozhin, V. Scardaci, Z. Sun, F. Hennrich, I. H. White, W. I. Milne, and A. C. Ferrari, "Wideband-tuneable, nanotube mode-locked, fibre laser," Nat. Nanotechnol. **3**(12), 738–742 (2008).
34. M. Zhang, E. J. R. Kelleher, F. Torrisi, Z. Sun, T. Hasan, D. Popa, F. Wang, A. C. Ferrari, S. V. Popov, and J. R. Taylor, "Tm-doped fiber laser mode-locked by graphene-polymer composite," Opt. Express **20**(22), 25077–25084 (2012).
35. F. Bonaccorso, Z. Sun, T. Hasan, and A. C. Ferrari, "Graphene photonics and optoelectronics," Nat. Photonics **4**(9), 611–622 (2010).
36. Z. Sun, T. Hasan, F. Torrisi, D. Popa, G. Privitera, F. Wang, F. Bonaccorso, D. M. Basko, and A. C. Ferrari, "Graphene Mode-Locked Ultrafast Laser," ACS Nano **4**(2), 803–810 (2010).
37. Z. Sun, D. Popa, T. Hasan, F. Torrisi, F. Wang, E. Kelleher, J. Travers, V. Nicolosi, and A. Ferrari, "A stable, wideband tunable, near transform-limited, graphene-mode-locked, ultrafast laser," Nano Res. **3**(9), 653–660 (2010).
38. J. S. Lauret, C. Voisin, G. Cassabois, C. Delalande, P. Roussignol, O. Jost, and L. Capes, "Ultrafast Carrier Dynamics in Single-Wall Carbon Nanotubes," Phys. Rev. Lett. **90**(5), 057404 (2003).

#191514 - $15.00 USD Received 30 May 2013; revised 29 Jul 2013; accepted 29 Jul 2013; published 24 Sep 2013

39. D. Brida, A. Tomadin, C. Manzoni, Y. J. Kim, A. Lombardo, S. Milana, R. R. Nair, K. S. Novoselov, A. C. Ferrari, G. Cerullo, and M. Polini, "Ultrafast collinear scattering and carrier multiplication in graphene," Nat Commun **4**, 1987 (2013).
40. A. Tomadin, D. Brida, G. Cerullo, A. C. Ferrari, and M. Polini, "Nonequilibrium dynamics of photoexcited electrons in graphene: Collinear scattering, Auger processes, and the impact of screening," Phys. Rev. B **88**(3), 035430 (2013).
41. F. Bonaccorso, A. Lombardo, T. Hasan, Z. P. Sun, L. Colombo, and A. C. Ferrari, "Production and processing of graphene and 2d crystals," Mater. Today **15**(12), 564–589 (2012).
42. V. Scardaci, Z. Sun, F. Wang, A. G. Rozhin, T. Hasan, F. Hennrich, I. H. White, W. I. Milne, and A. C. Ferrari, "Carbon Nanotube Polycarbonate Composites for Ultrafast Lasers," Adv. Mater. **20**(21), 4040–4043 (2008).
43. R. Going, D. Popa, F. Torrisi, Z. Sun, T. Hasan, F. Wang, and A. C. Ferrari, "500fs wideband tunable fiber laser mode-locked by nanotubes," Physica E **44**(6), 1078–1081 (2012).
44. R. B. Weisman and S. M. Bachilo, "Dependence of optical transition energies on structure for single-walled carbon nanotubes in aqueous suspension: An empirical Kataura plot," Nano Lett. **3**(9), 1235–1238 (2003).
45. H. Kataura, Y. Kumazawa, Y. Maniwa, I. Umezu, S. Suzuki, Y. Ohtsuka, and Y. Achiba, "Optical properties of single-wall carbon nanotubes," Synth. Met. **103**(1-3), 2555–2558 (1999).
46. E. Flahaut, C. Laurent, and A. Peigney, "Catalytic CVD synthesis of double and triple-walled carbon nanotubes by the control of the catalyst preparation," Carbon **43**(2), 375–383 (2005).
47. S. Osswald, E. Flahaut, H. Ye, and Y. Gogotsi, "Elimination of D-band in Raman spectra of double-wall carbon nanotubes by oxidation," Chem. Phys. Lett. **402**(4-6), 422–427 (2005).
48. S. Osswald, E. Flahaut, and Y. Gogotsi, "In Situ Raman Spectroscopy Study of Oxidation of Double- and Single-Wall Carbon Nanotubes," Chem. Mater. **18**(6), 1525–1533 (2006).
49. A. M. Rao, E. Richter, S. Bandow, B. Chase, P. C. Eklund, K. A. Williams, S. Fang, K. R. Subbaswamy, M. Menon, A. Thess, R. E. Smalley, G. Dresselhaus, and M. S. Dresselhaus, "Diameter-selective Raman scattering from vibrational modes in carbon nanotubes," Science **275**(5297), 187–191 (1997).
50. C. Fantini, A. Jorio, M. Souza, M. S. Strano, M. S. Dresselhaus, and M. A. Pimenta, "Optical Transition Energies for Carbon Nanotubes from Resonant Raman Spectroscopy: Environment and Temperature Effects," Phys. Rev. Lett. **93**(14), 147406 (2004).
51. H. Telg, J. Maultzsch, S. Reich, F. Hennrich, and C. Thomsen, "Chirality Distribution and Transition Energies of Carbon Nanotubes," Phys. Rev. Lett. **93**(17), 177401 (2004).
52. J. C. Meyer, M. Paillet, T. Michel, A. Moréac, A. Neumann, G. S. Duesberg, S. Roth, and J.-L. Sauvajol, "Raman Modes of Index-Identified Freestanding Single-Walled Carbon Nanotubes," Phys. Rev. Lett. **95**(21), 217401 (2005).
53. A. C. Ferrari and J. Robertson, "Interpretation of Raman spectra of disordered and amorphous carbon," Phys. Rev. B **61**(20), 14095–14107 (2000).
54. T. Hasan, V. Scardaci, P. Tan, A. G. Rozhin, W. I. Milne, and A. C. Ferrari, "Stabilization and "Debundling" of Single-Wall Carbon Nanotube Dispersions in N-Methyl-2-pyrrolidone (NMP) by Polyvinylpyrrolidone (PVP)," J. Phys. Chem. C **111**(34), 12594–12602 (2007).
55. F. Bonaccorso, T. Hasan, P. H. Tan, C. Sciascia, G. Privitera, G. Di Marco, P. G. Gucciardi, and A. C. Ferrari, "Density Gradient Ultracentrifugation of Nanotubes: Interplay of Bundling and Surfactants Encapsulation," J. Phys. Chem. C **114**(41), 17267–17285 (2010).
56. D. U. Noske, N. Pandit, and J. R. Taylor, "Source of spectral and temporal instability in soliton fiber lasers," Opt. Lett. **17**(21), 1515–1517 (1992).
57. E. M. Dianov, A. Y. Karasik, P. V. Mamyshev, A. M. Prokhorov, V. N. Serkin, M. F. Stelmakh, and A. A. Fomichev, "Stimulated-Raman Conversion of Multisoliton Pulses in Quartz Optical Fibers," JETP Lett. **41**, 294–297 (1985).
58. R. Hui and M. S. O'Sullivan, *Fiber optic measurement techniques* (Academic Press, 2009), xvii, 652 p.

1. Introduction

Over the past decade, supercontinuum sources in the near-infrared (IR), utilizing silica-based photonic crystal fibers (PCFs), have become a commercial success [1]. Typically, such systems are pumped by a master oscillator power fiber amplifier (MOPFA) [2, 3], employing ytterbium (Yb) doped fiber technology, and can cover the transparency window of silica (~0.35 – 2.2 μm [4, 5]), with high-average spectral power [2, 3, 6].

There is widespread interest in extending the long wavelength edge of the supercontinuum beyond the region where pure silica can be employed, for applications such as spectroscopy of trace gases [7], chemical kinetics [8] and military counter measures [9]. Progress in this regard has been made using fluoride [10, 11] and chalcogenide [12] glass fibers, in particular ZBLAN (**Z**rF_4-**B**aF_2-**L**aF_3-**Al**F_3-**N**aF) [10, 11, 13] and tellurite [14, 15] glasses, because of their enhanced transmission in the mid-IR [5, 10–16]. Step-index fibers fabricated from soft glasses, with transmission windows extending up to 5 μm, have been used to demonstrate supercontinua covering the 1 – 4 μm region [10, 11], pumped by high-power multi-stage erbium (Er) doped fiber lasers operating near the low anomalous dispersion region of the fiber

#191514 - $15.00 USD Received 30 May 2013; revised 29 Jul 2013; accepted 29 Jul 2013; published 24 Sep 2013

[10, 11]. An alternative approach targets the development of PCFs made from tellurite [14, 15], including short length tapers [5], because of their high nonlinear coefficients and broad mid-IR transparency [5, 14, 15].

While fluoride glass fibers have superior transmission beyond 2 μm compared to silica [10, 11], they are non-resistant to moisture [17] and, as such, degrade in air over time [5, 17]. In addition, poor compatibility with silica [5] reduces their potential for realizing fully fiber-integrated systems. Although chalcogenides are hydrophobic [18], consequently more stable against corrosion [5], the fabrication of compound glass fibers exhibiting single-mode performance is complex [5].

Germanium dioxide (GeO_2) is closely related chemically to silicon dioxide, sharing many properties that make it an excellent material for the manufacture of single-mode fibers [19], but with superior mid-IR transmission [19–21]. In addition, bulk GeO_2 glass has nearly an order of magnitude larger Raman scattering cross-section compared to bulk SiO_2 [19, 20] and a higher Kerr nonlinearity [19]. Consequently, GeO_2 doping of the core region is routinely used to enhance the Raman gain of conventional silica-based fibers [19–23]. Advances in fabrication techniques permit GeO_2 doping concentrations in excess of 50 mol. % [19], despite a mismatch in the thermal expansion coefficients of SiO_2 and GeO_2 [19, 20].

Recently, Raman-soliton continuum generation was demonstrated in a highly-doped GeO_2 silica-clad fiber, using an Er-based pump source [24, 25]. The bandwidth of the continuum exceeded 1000 nm, with the long-wavelength limit at 2.5 μm [24, 25]. Extension of the infrared edge of the continuum can be achieved using a longer wavelength pump source [26, 27]. Examples of suitable pump systems include: broadly tunable, ultrashort pulse optical parametric amplifiers (OPAs) and optical parametric oscillators (OPOs) [25–28] and, more recently [13], thulium-(Tm) doped fiber-based systems [13]. OPAs and OPOs, however, are complex and expensive systems and cannot deliver the benefit of a compact design, efficient heat dissipation, and alignment-free operation offered by fiber lasers [5].

Ultrafast sources based on Tm-doped fibers operating around 2 μm are becoming increasingly important to address demands for mid-IR sources [5]. Tm-based mode-locked oscillators have previously been reported employing nonlinear polarization rotation (NPR) and semiconductor saturable absorber mirrors (SESAMs) [5]. NPR and SESAMs, however, can suffer from environmental sensitivity or require complex fabrication [5]. Carbon nanotubes (CNTs) [28–33] and graphene [29, 31, 34–37], have emerged as alternative saturable absorbers (SA) with ultrafast recovery time [38–40], able to support short pulses, and with a number of favorable properties, such as broadband operation [34, 38], and ease of fabrication [31, 35, 41] and integration [30] into all-fiber configurations. While broadband operation is an intrinsic property of graphene [35], in CNTs this can be achieved using a distribution of tube diameters [34]. A variety of techniques have been implemented in order to integrate CNTs and graphene into lasers [29]. CNTs and graphene embedded in polymer matrices can be easily integrated into a range of photonic systems [31, 35]. CNTs can be homogeneously embedded into polymer matrices, resulting in high quality composites [31, 42], exhibiting large modulation depths [30, 33, 42, 43], preferred for fiber lasers [5].

Here, we report the generation of a Raman-soliton continuum, extending beyond 2.5 μm, pumped at 1.95 μm with 12 kW peak power pulses delivered from a nanotube-mode-locked Tm-based MOPFA, in an optimized 3.4 m length of 75 mol. % GeO_2 fiber. We use CNTs with diameter ~1.7 nm, in order to achieve a strong absorption in the:2 μm range [44, 45]. The CNTs are embedded in a polymer matrix, thus forming our SA to mode-lock the seed laser of the MOPFA. This approach provides a robust, long-term stable source of radiation in an important band, coincident with a portion of the atmospheric transmission window.

2. Seed laser

The schematic of the seed oscillator is shown in Fig. 1. This consists of all-fiber integrated components, in order to have an environmentally stable and compact system. A Tm–doped fiber amplifier, with integrated optical isolator (ISO), provides a peak small signal gain of ~25 dB at 1.94 μm, with gain available over a broad bandwidth (full width at half maximum,

#191514 - $15.00 USD Received 30 May 2013; revised 29 Jul 2013; accepted 29 Jul 2013; published 24 Sep 2013

FWHM ~60 nm), suitable to support the generation of short pulses. A fiber pigtailed air-gap (20% insertion loss) is used to include an intra-cavity band-pass filter (BPF) for pulse stabilization, with 80% maximum transmission and 11 nm bandwidth, centered at ~1.94 μm. The output signal is delivered through a 30:70 fiber coupler. A polarization controller (PC) allows continuous adjustment of the intra-cavity polarization state.

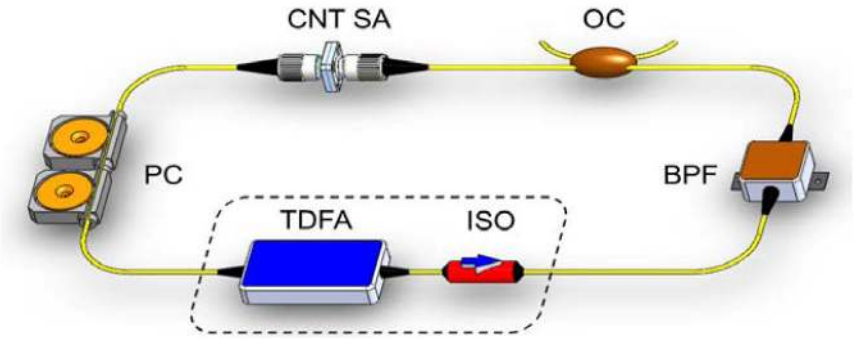

Fig. 1. Schematic of the mode-locked oscillator. TDFA: thulium-doped fiber amplifier, ISO: isolator, BPF: bandpass filter, OC: fiber output coupler, CNT SA: carbon nanotube saturable absorber, PC: polarization controller.

The SA is designed to have absorption coincident with the operating wavelength of the oscillator, centered at 1.94 μm. We use CNTs produced by Catalytic Chemical Vapor Deposition (CCVD) of CH_4 over $Mg_{1-x}Co_xO$ solid solution containing Mo oxide [46]. The catalyst and byproducts are dissolved by treatment with concentrated aqueous HCl solution [46]. The remaining carbon-encapsulated catalytic nanoparticles are removed by air oxidation at 450°C for 1 h in an open furnace, followed by HCl washing to dissolve metal oxides formed during the oxidation step [47, 48]. In order to further purify the sample, oxidation in air at higher temperature (570°C) is carried out for a shorter time (30 min) [48]. The residual material is further washed with HCl to dissolve the remaining metal oxides [47, 48].

The absorption spectrum of the purified CNTs is shown in Fig. 2(a) (black line) with a peak between 1.75 and 2.15 μm. The desired operating wavelength is also highlighted (red dashes). To further investigate their optical proprieties, we also measure the Raman spectra of the purified CNTs powder at 457 (2.71 eV), 514.5 (2.41 eV), and 632.8 nm (1.96 eV). In the low frequency region, the Radial Breathing Modes (RBMs) are observed [48]. Their energy is inversely related to CNT diameter, d_t [50–52] by the relation $\omega_{RBM} = C_1 / d_t + C_2$. We use C_1 = 214.4 cm^{-1} and C_2= 18.7 cm^{-1} from Ref [51]. These were derived in Ref [51] by plotting the resonance energy as a function of inverse RBM frequency without any additional assumptions. However, we also validated our results by using the parameters proposed in Refs [50, 52]. For all excitation wavelengths and samples analyzed, we found a maximum discrepancy of 0.03 nm on the tube diameter. The RBM spectra of the powders [Fig. 2(c)] (black lines) show a broad diameter distribution, spanning the 140–377 cm^{-1} range. This corresponds to CNTs with ~0.6-1.8 nm diameter. Figure 2(d) plots the Raman spectra in the *G* region of purified CNTs (black curves). A weak *D* band is observed [I(D)/I(G) = 0.04], indicating small number of defects [53].

#191514 - $15.00 USD Received 30 May 2013; revised 29 Jul 2013; accepted 29 Jul 2013; published 24 Sep 2013

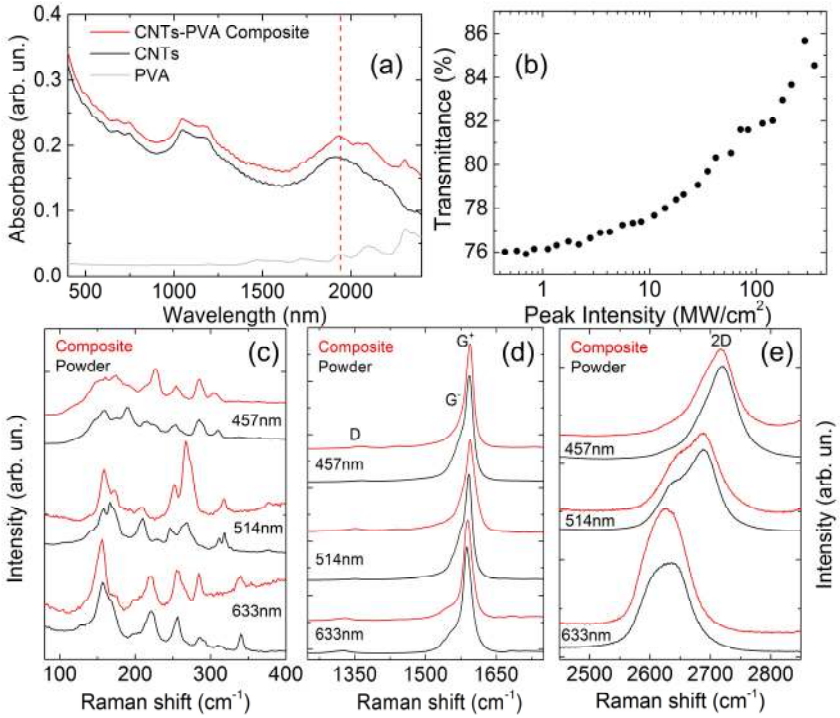

Fig. 2. (a) Absorption spectrum of CNTs (black line), CNT-PVA composite (red line), and PVA (grey line). The operating wavelength is marked by the red dashed line. (b) Transmittance as a function of peak intensity. Raman spectra of CNT powders (black lines) and CNT-PVA composite (red lines) at different excitation wavelengths: (c) RBM region, (d) G region, (e) 2D region.

A polymer composite is then fabricated via solution processing [30–33, 42]. Purified CNTs are dispersed using a tip sonicator (Branson 540 A, 20kHz) in water with sodium dodecylbenzene sulfonate (SDBS) as surfactant for 4 h. The dispersion is then ultracentrifuged (Sorvall WX Ultra) at 100,000 *g*, where *g* is the gravitational acceleration, for 30 mins. The top 70% dispersion, free from insoluble particles and CNT aggregates, is then decanted. 4 ml are mixed with 120 mg polyvinyl alcohol (PVA) and ultrasonicated again for 30 mins, obtaining a homogeneous and stable dispersion. We use water as the solvent, due to its low boiling point compared to common organic solvents used to disperse CNTs, such as N-Methyl Pyrrolidone (NMP) [31] with a boiling point of 206° C [54]. SDBS is used as the surfactant for its ability to produce small CNT bundles [55], unlike bile salts, *e.g.* sodium cholate, more effective in the dispersion of individual nanotubes [55]. PVA is used for its compatibility with water [31]. The CNT-polymer mixture is drop-cast in a petri dish. Slow evaporation, over 4-5 days at room temperature in a desiccator, produces a free-standing ~50 μm composite. The concentration, *c*, of CNTs in the PVA film is estimated to be ~0.3 weight percent (wt%), derived by measuring the weight of the decanted CNT dispersion compared to that of the solution × 100%.

Figure 2(a) plots the absorption spectra of the PVA (grey line), the CNT-PVA composite (red line) and the pristine CNTs (black line). The absorption of the PVA is ~1 order of magnitude lower with respect to the CNT-PVA composite, in the 400 – 2000 nm range, thus negligible. The absorption band between 1.75 and 2.15 μm corresponds to eh11 excitonic transitions of tubes with diameters in the 1.5–1.8 nm range [43, 44]. Power-dependent absorption is measured with an optical parametric oscillator (Coherent, Chameleon) delivering ~260 fs pulses with 80 MHz repetition rate at 1945 nm. The optical transmittance is determined by monitoring the input and output power on the CNT composite. The

#191514 - $15.00 USD Received 30 May 2013; revised 29 Jul 2013; accepted 29 Jul 2013; published 24 Sep 2013

nonlinear transmittance increases from ~76% to ~85%, Fig. 2(b), giving a ~9% change in transmittance, comparable that typically reported for CNTs [32, 41, 42]. We also measured the Raman spectra of the composite and, for the three excitation wavelengths, we do not observe any change in the RBM distribution with respect to the pristine CNTs. Thus, the dispersion process and the CNT-PVA composite fabrication do not induce additional defects [52] with respect to the starting material.

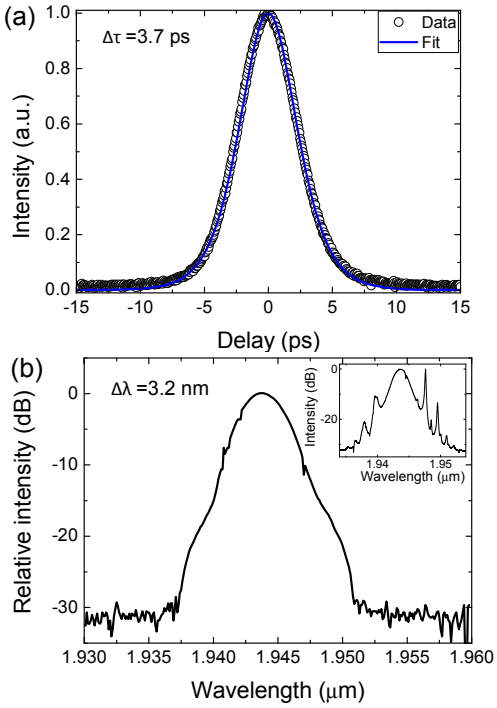

Fig. 3. Seed laser performance. (a) Autocorrelation of the output pulses, with a deconvolved duration of 3.7 ps. (b) The corresponding optical spectrum (high resolution, inset).

The CNT-SA is then inserted between two SMF-28 fiber connectors and directly fusion spliced into the laser cavity. The oscillator operates at the fundamental repetition frequency of the cavity, 6.1 MHz, and produces 3.5 mW average output power, corresponding to 0.57 nJ single pulse energy. The autocorrelation of the output pulses and the corresponding optical spectrum are plotted in Fig. 3. The autocorrelation is well fitted by a *sech*^{2} pulse-shape, with a 3.7 ps deconvolved FWHM duration, Fig. 3(a). The optical spectrum, shown in Fig. 3(b) and recorded using an automated grating spectrometer, is centered at 1.94 μm with a 3.2 nm FWHM. The seed spectrum is also recorded using a long wavelength range optical spectrum analyzer (Yokogawa). This allows us to observe solitonic spectral sidebands (Fig. 3(b) inset). The overall cavity group velocity dispersion (GVD) can be estimated from the spectral sideband separation [56] $\Delta\lambda = \pm \frac{\lambda^2}{2\pi c}\frac{\tau}{1.763}\sqrt{-1+\frac{8z_0}{z_A}}$, where τ [s] is the pulse duration, λ [m] is the peak wavelength, $z_0 = \frac{\pi}{2}\frac{\tau^2}{\beta_2}$ [s·m] is the soliton period with β_2 [s/m] the GVD coefficient and z_A [m] the cavity length. Thus, $\beta_2 = \frac{\pi\tau^2}{2z_0}$ = –69.2 ps^2 km^{-1} is estimated.

#191514 - $15.00 USD Received 30 May 2013; revised 29 Jul 2013; accepted 29 Jul 2013; published 24 Sep 2013

3. Tm-doped MOPFA and supercontinuum generation

The configuration of the system for supercontinuum generation is shown in Fig. 4. Prior to amplification, the output pulses from the seed oscillator are temporally stretched to greater than 80 ps through dispersive broadening in a 1.2 km single-mode silica fiber, with normal GVD~34 $ps^2\ km^{-1}$ at 1.95 μm, in order to reduce the peak power.

The amplifier is constructed from 5.5 m single-mode Tm-doped fiber (Nufern SM-TSF-9/125), pumped through a fiber wavelength division multiplexer (WDM) by a 7 W continuous-wave (CW) Er laser. The lengths of active fiber and pump power are optimized to preserve pulse quality during amplification, so to maximize the signal gain. A second WDM at the output of the amplifier extracts residual pump light. Figure 5(a) shows the autocorrelation trace of the amplified output, under maximum pump power, corresponding to an average signal power of 150 mW. Again, a $sech^2$ fit well represents the pulse-shape, with ~80 ps duration. The pulse spectrum [Fig. 5(b)] is centered at 1.95 μm and has a 6.2 nm FWHM. A pump power of 7 W is required because the seed line is not coincident with the peak of the spontaneous fluorescence spectrum of the active fiber used in the amplifier, limiting the available gain at 1.95 μm.

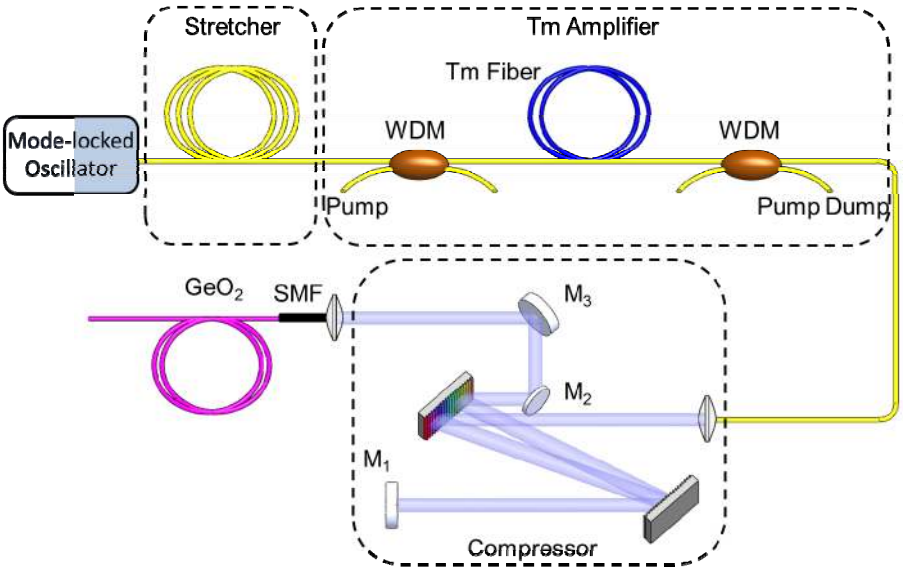

Fig. 4. Schematic of the Tm-fiber system for pulse amplification, compression and supercontinuum generation. WDM: wavelength division multiplexer. Mirror M_1 is tilted to separate the outgoing beam from the incoming beam. Mirror M_2 reflects the compressed pulses output without introducing any additional losses. M_1, M_2, and M_3 are highly reflective broadband mirrors.

To achieve a kW level peak power, the pulses are recompressed by collimating the output through an aspheric lens and double passing a pair of 800 lines/mm gold coated gratings, optimized to operate in the 1.8 – 2.2 μm range. Through adjustment of the grating separation, 850 fs FWHM duration is achieved [Fig. 6(a)]. No pedestal component is observed, indicating high quality amplification and compression. The low-level satellite pulses are assigned to residual nonlinear chirp accumulated in the long-length stretcher stage, to the amplification process, and to uncompensated third order dispersion. Figure 6(b) shows the largely unchanged spectrum after compression. 10 cm of SMF is used as an intermediate fiber, to facilitate improved coupling to the GeO_2 fiber. Repeatable splice loss between the GeO_2 and SMF fiber is as low as 0.4 dB (i.e. ~8.8%). The zero dispersion wavelength (ZDW) of the GeO_2 fiber (i.e. the wavelength where the group delay dispersion of a fiber is zero [5]) shifts with the doping concentration, such that at a 75 mol. % this is expected to be in the 1.8 – 1.9

#191514 - $15.00 USD Received 30 May 2013; revised 29 Jul 2013; accepted 29 Jul 2013; published 24 Sep 2013

μm range [21]. Thus, here we pump in the region of low anomalous GVD and expect continuum dynamics initiated by modulation instability (MI), given the pump format. This explanation of the dynamics [57] is consistent with the fact that the spectral sideband signature of MI is observed at low pump powers, before significant continuum formation.

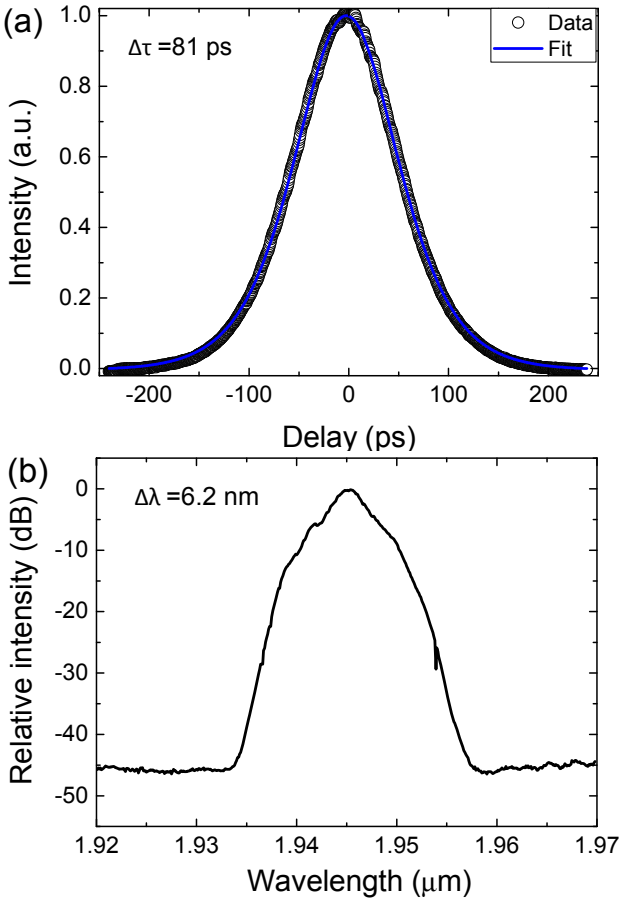

Fig. 5. MOPFA results. (a) Autocorrelation of the amplified pulses with 81 ps duration. (b) Corresponding optical spectrum.

Spectral measurements after the GeO_2 fiber are taken using an automated Spex 500 spectrometer in combination with a PbS IR detector and lock-in amplifier. Although the transmission of GeO_2 is superior to silica beyond ~2.1 μm, the loss at wavelengths longer than 2.5 μm still increases significantly to hundreds of dB km^{-1} [20]. As such, it is important to pump short lengths, with high-peak power pulsed sources. Note that this limits the application of CW lasers as a suitable pump source in this case, thus high-average spectral power continuum sources in this wavelength range remain a challenge.

The average spectrum is recorded as a function of fiber length using a cutback technique [58] starting from a 5.6 m GeO_2 fiber. A plot of the corresponding generated supercontinuum bandwidth (10 dB level) as a function of fiber length is shown in Fig. 7. The continuum width monotonically decreases beyond ~3.5 m, which can be attributed to re-absorptive loss due to infrared absorption [20]. The broadest spanning supercontinuum achieved, where a balance of nonlinear gain and linear loss is reached, is shown in Fig. 8. A spectrum extending from 1.9 to 3 μm is generated in an optimized fiber length of 3.4 m.

#191514 - $15.00 USD Received 30 May 2013; revised 29 Jul 2013; accepted 29 Jul 2013; published 24 Sep 2013

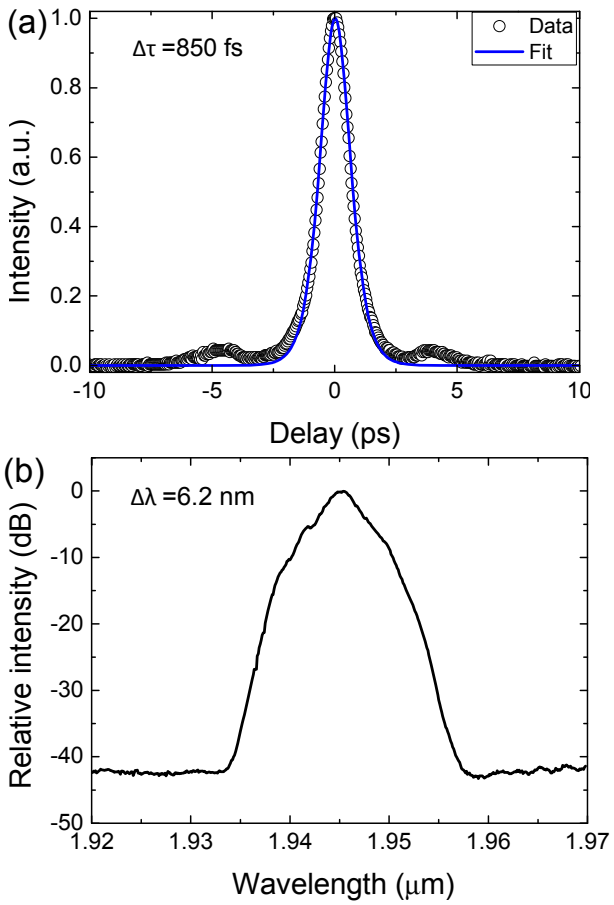

Fig. 6. (a) Autocorrelation of the compressed pulses, with an 850 fs duration. (b) Corresponding optical spectrum.

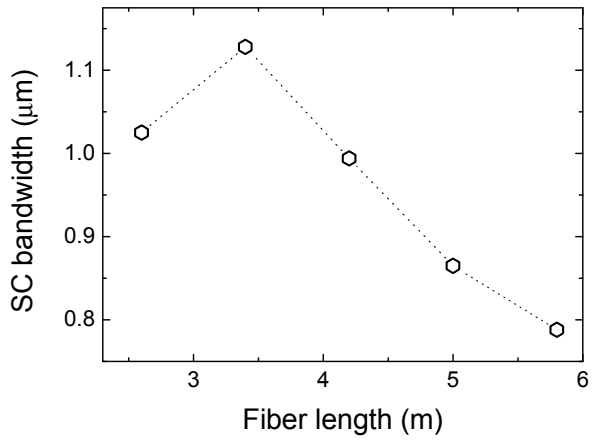

Fig. 7. Supercontinuum bandwidth (10 dB) as a function of GeO_2 fiber length.

#191514 - $15.00 USD Received 30 May 2013; revised 29 Jul 2013; accepted 29 Jul 2013; published 24 Sep 2013

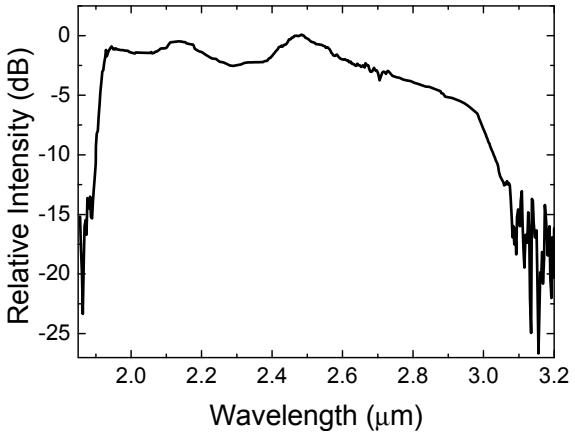

Fig. 8. Output spectrum after 3.4 m of propagation in the GeO_2 fiber.

4. Conclusions

We demonstrated the generation of a Raman-soliton continuum, extending from 1.9 to 3 μm in an optimized 3.4 m length of 75 mol. % GeO_2 fiber, and pumped at 1.95 μm by a Tm-based MOPFA delivering 12 kW peak power, sub-picosecond pulses. This robust and simple fiber system addresses an important region beyond the long wavelength extent of common pure-silica PCF-based supercontinuum light sources.

Acknowledgments

We thank Dr. V.F. Khopin and Prof. A.N. Guryanov (Institute of Chemistry of High-Purity Substances of the Russian Academy of Sciences) for the germanate-glass-core fiber fabrication. We acknowledge funding from a Royal Society Wolfson Research Merit Award, the ERC Grant NANOPOTS, EPSRC grants EP/K01711X/1, EP/K017144/1, the Newton Trust, the Newton International Fellowship, and Emmanuel College, Cambridge.